OPTICAL REVIEW Vol. 17, No. 5 (2010) 467–475

Chaos Synchronization in Semiconductor Lasers with Polarization-Rotated Optical Feedback

Yasutoshi TAKEUCHI, Rui SHOGENJI[1], and Junji OHTSUBO[1]*

Graduate School of Engineering, Shizuoka University, Hamamatsu 432-8561, Japan
[1]*Faculty of Engineering, Shizuoka University, Hamamatsu 432-8561, Japan*

(Received April 28, 2010; Accepted July 5, 2010)

Chaotic oscillations of the transverse magnetic (TM) mode, which is not a common lasing mode, are excited by using polarization-rotated optical feedback from the transverse electric (TE) mode in a semiconductor laser. In our previous paper, we found that the dynamics were strongly dependent on their RF components under the condition of moderate optical feedback from the TE mode to the TM mode and that they were divided into three RF regions; low-pass filtered signals with a lower frequency than the laser relaxation oscillation frequency, intermediate RF components including the relaxation oscillation frequency, and high-pass filtered signals with a higher frequency higher than the relaxation oscillation frequency. Depending on the frequency bands, the laser outputs showed different correlations. In the present study, using such schemes, the polarization-rotated beam from a transmitter laser (i.e., the rotated TE-mode beam of a transmitter laser) is injected into a receiver laser. We experimentally observe chaos synchronization in accordance with the dynamics of RF components on the transmitter laser side. We also perform numerical calculations using a model and obtain good agreement between the theoretical and experimental results.

Keywords: semiconductor laser, optical feedback, polarization, chaos synchronization

1. Introduction

Chaotic systems in semiconductor lasers with optical feedback are used as transmitters and receivers in chaotic secure communications, since they enable a very fast communication channel to be constructed.[1)] In general, an edge-emitting semiconductor laser oscillates in a transverse electric (TE) mode and TE optical feedback is employed as a chaotic transmitter.[2,3)] An alternative scheme is polarization-rotated optical feedback, in which the polarization of the TE mode is rotated by 90° and the rotated beam is fed back to the transverse magnetic (TM) mode in the laser cavity.[4–16)] In the dynamics of polarization-rotated optical feedback, we find different correlations between the chaotic oscillations than those found in previous studies.[16,17)] In previous studies, the dynamics were strongly dependent on their RF components and they were divided into three RF regions. For low-pass filtered signals with a lower frequency than the laser relaxation oscillation frequency, there is an antiphase correlation between the two polarization modes. On the other hand, the two polarization modes have an in-phase correlation for the RF components of high-pass filtered signals, which have a higher frequency than the relaxation oscillation frequency. However, no correlations are observed between the two modes for the intermediate RF components that include the relaxation oscillation frequency.

Chaos synchronization, which is the key to achieving chaotic secure communications, has been successfully demonstrated in a system with TE optical feedback in a transmitter semiconductor laser and TE optical injection into a receiver laser.[1–3)] A system with TE–TM polarization-rotated optical feedback and injection can also be applied to chaos synchronization.[8–13)] Indeed, using a chaotic oscillator with polarization-rotated optical feedback, chaos synchronization has been investigated for both perfect and injection-locking schemes.[10–13)] For example, in ref. 11, in-phase chaos synchronization between transmitter and receiver lasers was experimentally demonstrated within range of up to 6 GHz for strong optical feedback. However, the chaos synchronization properties for moderate polarization optical feedback and injection have not been studied.

In this paper, we experimentally and numerically study chaos synchronization in a system with polarization-rotated optical feedback and polarization-rotated optical injection under moderate optical feedback and optical injection ratios. In accordance with the previous result of the strong dependence of the dynamics on the RF component in the transmitter laser, we find similar results for chaos synchronization in the system. We perform numerical simulations using a model with rate equations and obtain good agreement between the theoretical and experimental results.

2. Experimental Setup

Figure 1 shows the experimental setup for chaos synchronization. The transmitter laser was that used in the previous experiment.[17)] The same two semiconductor lasers were used for the master (transmitter) laser (ML) and slave (receiver) laser (SL). The transmitter laser was a single-mode multi-quantum-well laser (Hitachi HL7851G) that oscillated at a wavelength of 783 nm and had a maximum power of 50 mW. The transmitter laser had a threshold current of 41.0 mA at a temperature of 25.0 °C. The laser mainly oscillated at a single TE mode under the operating conditions and the orthogonal TM mode was scarcely detectable in the case of solitary oscillation. The transmitter laser was biased at

*E-mail address: tajohts@ipc.shizuoka.ac.jp

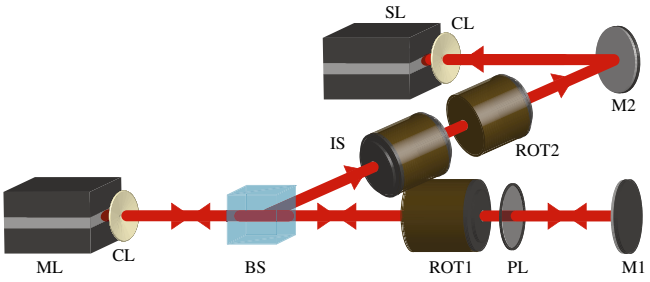

Fig. 1. (Color online) Experimental setup. ML: master transmitter laser, SL: slave receiver laser, CL: collimating lens, BS: beam splitter, ROTs: Faraday rotators, PL: polarizer, Ms: mirrors, IS: isolator.

70 mA, which corresponds to an injection current density of $1.7J_{\mathrm{th}}$ (J_{th} being the threshold injection current density). Under these operating conditions, the relaxation oscillation frequency, which plays an important role in the laser dynamics, was about 3.5 GHz. Using a Faraday rotator (ROT1) and a polarizer (PL), the polarization rotation of 90° (from TE to TM mode) was realized and a single feedback loop was always guaranteed in this setup.[16,17] The external cavity was about 30 cm long, which corresponds to a feedback time of 2.0 ns. The external intensity feedback ratio from the TE to TM optical power counted in the external loop was 13%. However, the actual feedback intensity to the laser cavity was roughly estimated to be less than 1/10th of the external fraction in our case (approximately 1%) due to the reflection and diffraction losses of the optical components.[17] We took into account the frequency detuning between the TE mode and the excited TM mode, which was encountered in the experiment. The observed frequency detuning was −870 MHz. Although this frequency detuning is small, theoretical analysis has demonstrated that nonzero frequency detuning plays an important role in the daynamics.[17] Under these feedback conditions, the power ratio between the TE- and TM-mode oscillations was 1000 : 7.

The slave receiver laser was the same type as the transmitter laser and it was biased at 69.5 mA at a temperature of 24.5 °C. This corresponds to almost the same bias injection ratio as the transmitter laser, and the relaxation oscillation frequency of the solitary mode was also about 3.5 GHz. The beam of the TE mode from the transmitter laser was divided by a beam splitter (BS) and passed through an isolator (IS) and another Faraday rotator (ROT2), then the 90°-polarization-rotated beam (in the direction of the TM mode in the receiver laser) was injected into the receiver laser. This configuration consists of unidirectional optical injection and an open-loop system for chaos synchronization. The injection ratio from the transmitter to the receiver laser was 7.8%. The transmission time of light from the transmitter to the receiver was 5 ns. Frequency detuning between the TE mode of the transmitter laser and the TM mode of the receiver laser was 2.10 GHz. The frequency detuning between the polarization modes within the receiver laser was −870 MHz.

In the experiments, we carefully selected two lasers for the transmitter and receiver, since the performance of chaos synchronization is strongly dependent on the parameter mismatches of not only variable external parameters (such as injection current, temperature, etc.) but also the intrinsic parameters of each device at the material level. The two lasers used in the experiments orignated from the same wafer and the intrinsic parameter errors of the devices were small enough to perform chaos synchronization.[1)] Thus, we can expect good chaos synchronization between the two lasers under appropriate experimental conditions. We also chose the same frequency detuning between the TE and TM modes for the transmitter and receiver lasers. The frequency detuning is dependent on each device and it is also varied by varying the bias injection current and temperature. However, the dependences of the detuning on the bias injection current and temperature are very small and the detuning is almost completely determined by the material parameters and device structures. It may not be easy to markedly change the frequency detuning by the control of external parameters in a real experiment, but a real semiconductor laser indeed has nonzero frequency detuning between the two polarization modes. This fact plays an important role in the dynamics as we will discuss in the following.

Although not shown in the figure, the transmitter and receiver laser beams were detected by photodetectors (PDs; New Focus 1554-50; bandwidth: 12 GHz) and were analyzed by a digital oscilloscope (Agilent DSO80804B; analogue bandwidth: 8 GHz, sampling rate: 40 GSa/s). The digital oscilloscope had a sufficiently large frequency bandwidth to observe fully chaotic dynamics including the typical laser relaxation oscillation. The laser oscillations were monitored by an optical spectrum analyzer (Advantest Q8344A; maximum resolution: 0.05 nm) and a Fabry–Perot spectrometer (Coherent Model 240; free spectral range: 7.5 GHz).

3. Experimental Results

Here we experimentally investigate the properties of chaos synchronization in the system. Figure 2(a) shows an example of chaotic waveforms for the TE modes of the transmitter and receiver lasers with the entire frequency bandwidth between 0 and 8 GHz when the corresponding low-pass filtered signals exhibit synchronous oscillations. The corresponding spectra in Fig. 2(b) show chaotic oscillations and a periodic component related to the external optical feedback loop. The relaxation oscillation component at approximately 3.5 GHz is greatly enhanced in the receiver laser. Figure 2(c) shows the correlation between the two waveforms of the TE modes in Fig. 2(a). We use the same definition of the intensity correlation function $C(T)$ as that in the previous paper,[16,17] where T is the time lag of the correlation. The time required for optical injection from the transmitter to the receiver laser is 5 ns, so that a small peak is observed at this delay ($T = -5$ ns). However, the peak is not large and the correlation is weak. Also, small periodic peaks are visible that correspond to the separation for the optical feedback of 2 ns. The correlation plot in Fig. 2(d) reveals no distinct relationship between the two modes at a time delay of $T = -5$ ns.

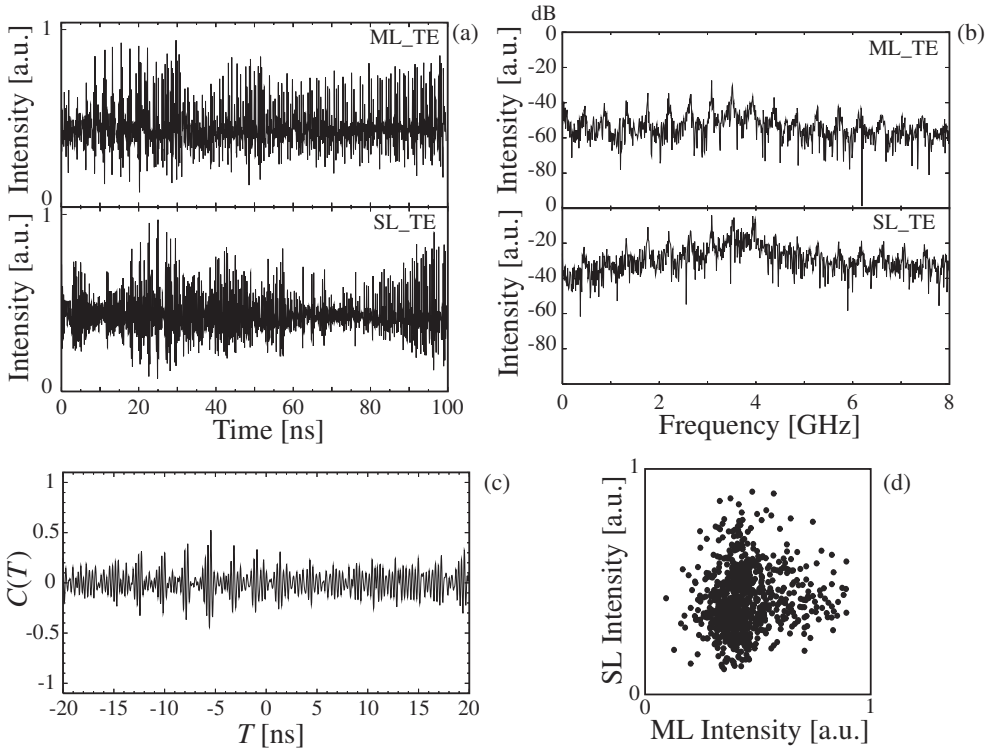

Fig. 2. Experimental results for chaos synchronization. (a) Time series of chaotic TE waveforms in transmitter and receiver lasers over the entire frequency bandwidth (0–8 GHz). (b) Corresponding RF spectra. (c) Correlation between the two waveforms of the TE mode in (a), and (d) correlation plot at $T = -5$ ns.

On the other hand, different dynamics are observed for the chaotic signals depending on the RF components. We used the same three RF bands as those in the previous section. In Fig. 3, the left column shows the results for the low-pass filtered signals. A large negative correlation peak is clearly visible at $T = -5$ ns in Fig. 3(b). Figure 3(c) shows the correlation plot at $T = -5$ ns and the correlation coefficient is $C(-5) = -0.713$. Figure 3(e) shows the correlation for the band-pass filtered signals. No tendency is visible for the correlation plot at $T = -5$ ns in Fig. 3(f). Also, there is no clear correlation for the high-pass filtered signals in Figs. 3(h) and 3(i). However, it may be difficult to draw definite conclusions from the evaluation of the correlations in Figs. 3(h) and 3(i) in the current experiment. This is for the same reason as that given in the previous experiment:[17] namely, the experimentally excited TM mode on the receiver side is very small, especially at the higher frequency component. Thus, the intensity of the high-pass filtered TM-mode signal is very low and the TM-mode oscillation in the receiver laser is almost the same level as the noise in the semiconductor laser. The TE mode of the receiver laser may not be fully excited by the drive signal.

Figure 4 shows the correlations between the TE and TM modes within the receiver laser under the same conditions as those for Fig. 3. The entire frequency bandwidth shows no correlation between the two modes. However, a clear antiphase oscillation is visible for the low-pass filtered signals. The two modes oscillate in an antiphase manner with zero time delay ($T = 0$ ns), as shown in Fig. 4(d), and the correlation coefficient is $C(0) = -0.769$. Although not shown in this paper, the band- and high-pass filtered signals exhibit no correlation at $T = 0$ ns.

4. Theory

We conducted numerical simulations by employing the rate equations for the experimental model. The rate equations for the complex fields E and the carrier density n for the master transmitter laser with polarization-rotated optical feedback are given by

$$\frac{dE_{\mathrm{ML\_TE}}(t)}{dt} = \frac{1}{2}(1 - i\alpha)G_{n,\mathrm{ML\_TE}}\{n_{\mathrm{ML}}(t) - n_{\mathrm{th,ML\_TE}}\}E_{\mathrm{ML\_TE}}(t), \tag{1}$$

$$\frac{dE_{\mathrm{ML\_TM}}(t)}{dt} = \frac{1}{2}(1 - i\alpha)G_{n,\mathrm{ML\_TM}}\{n_{\mathrm{ML}}(t) - n_{\mathrm{th,ML\_TM}}\}E_{\mathrm{ML\_TM}}(t) + \frac{\kappa}{\tau_{\mathrm{in}}}E_{\mathrm{ML\_TE}}(t-\tau)\exp\{i(-\Delta\omega_{\mathrm{ML}}t + \omega_{\mathrm{ML\_TE}}\tau)\}, \tag{2}$$

$$\frac{dn_{\mathrm{ML}}(t)}{dt} = \frac{J_{\mathrm{ML}}}{ed} - \frac{n_{\mathrm{ML}}(t)}{\tau_{\mathrm{s}}} - \{n_{\mathrm{ML}}(t) - n_0\}\{G_{n,\mathrm{ML\_TE}}|E_{\mathrm{ML\_TE}}(t)|^2 + G_{n,\mathrm{ML\_TM}}|E_{\mathrm{ML\_TM}}(t)|^2\}, \tag{3}$$

$$\Delta\omega_{\mathrm{ML}} = \omega_{\mathrm{ML\_TE}} - \omega_{\mathrm{ML\_TM}} = 2\pi(f_{\mathrm{ML\_TE}} - f_{\mathrm{ML\_TM}}), \tag{4}$$

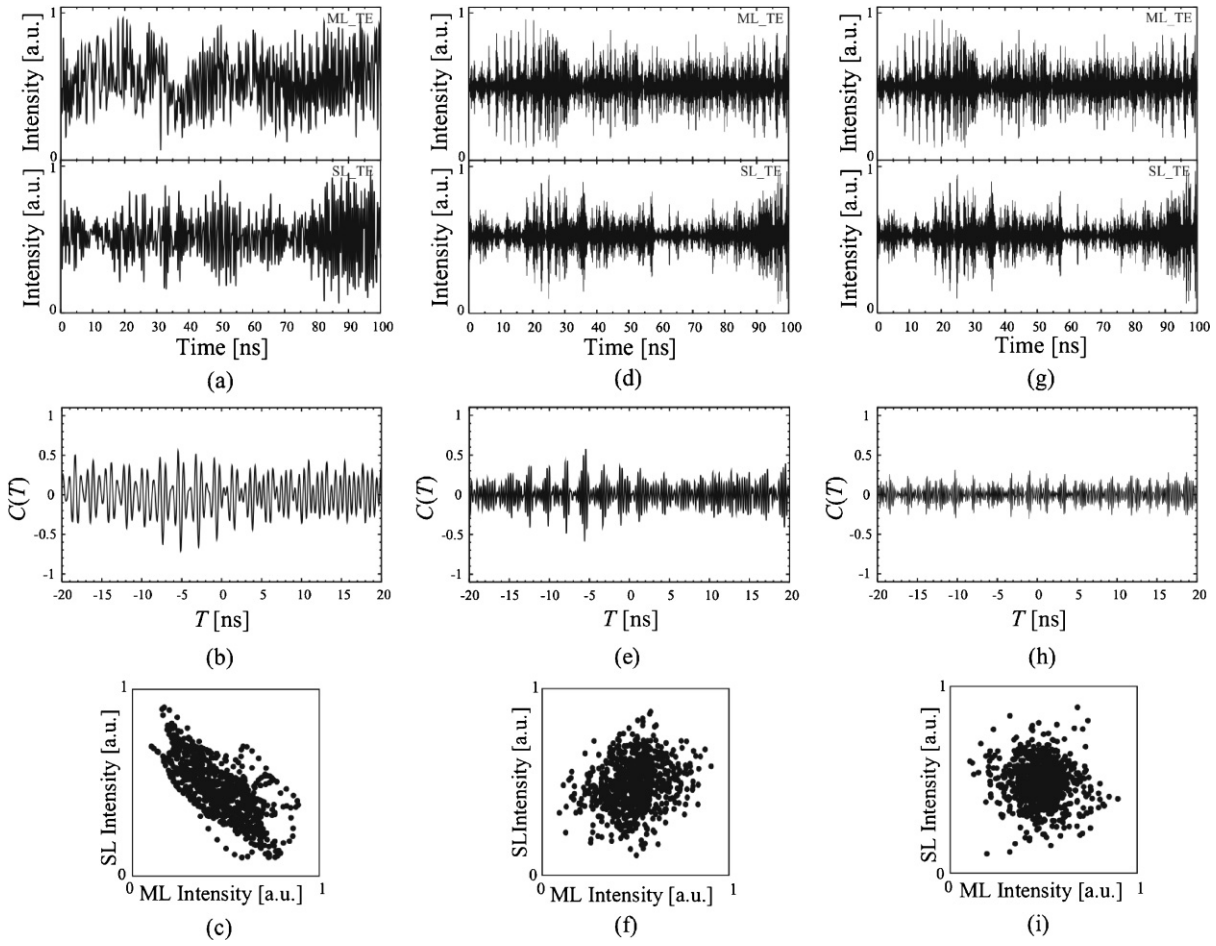

Fig. 3. Experimental results for RF-band-limited waveforms and correlations in transmitter and receiver lasers. Left column: low-pass filtered results (0–2 GHz). Middle column: band-pass filtered results (2.0–4.5 GHz). Right column: high-pass filtered results (4.5–8 GHz). Upper row: Time series of TE modes. Middle row: Correlation between the waveforms of the upper row. Bottom row: Correlation plot at $T = -5$ ns.

where the subscript ML indicates the master transmitter laser, and the additional subscripts TE and TM represent the variables and parameters for the TE and TM modes, respectively. In eq. (2), the second term on the right-hand side is the effect of time-delayed orthogonal polarization-rotated optical feedback. n_{th} and G_n are the threshold carrier densities and the gain coefficients, respectively. In the following numerical simulations, we take into account the gain difference but we assume that the threshold carrier densities are equal.[15] α, κ, and τ_{in} are the linewidth enhancement factor, the feedback coefficient, and the round trip time within the internal cavity, respectively. τ is the round-trip time of light in the external optical feedback. $\Delta\omega_{\mathrm{ML}}/2\pi$ is the frequency detuning between the two polarization modes ($f_{\mathrm{ML\_TE}}$ and $f_{\mathrm{ML\_TM}}$ being the laser frequencies for the TE and TM modes, respectively). J is the bias injection current density. τ_{s} and n_0 are the carrier lifetime and the carrier number at transparency, respectively, and e and d are the elemental charge and the thickness of the active layer, respectively.

The complex fields and the carrier density equations for the slave receiver laser are given by

$$\frac{dE_{\mathrm{SL\_TE}}(t)}{dt} = \frac{1}{2}(1 - i\alpha)G_{n,\mathrm{SL\_TE}}\{n_{\mathrm{SL}}(t) - n_{\mathrm{th,SL\_TE}}\}E_{\mathrm{SL\_TE}}(t), \tag{5}$$

$$\frac{dE_{\mathrm{SL\_TM}}(t)}{dt} = \frac{1}{2}(1 - i\alpha)G_{n,\mathrm{SL\_TM}}\{n_{\mathrm{SL}}(t) - n_{\mathrm{th,SL\_TM}}\}E_{\mathrm{SL\_TM}}(t) + \frac{\kappa_{\mathrm{inj}}}{\tau_{\mathrm{in}}}E_{\mathrm{ML\_TE}}(t - \tau_{\mathrm{c}})\exp\{i(-\Delta\omega_{\mathrm{inj}}t + \omega_{\mathrm{ML\_TE}}\tau_{\mathrm{c}})\}, \tag{6}$$

$$\frac{dn_{\mathrm{SL}}(t)}{dt} = \frac{J_{\mathrm{SL}}}{ed} - \frac{n_{\mathrm{SL}}(t)}{\tau_{\mathrm{s}}} - \{n_{\mathrm{SL}}(t) - n_0\}\{G_{\mathrm{SL\_TE}}|E_{\mathrm{SL\_TE}}(t)|^2 + G_{\mathrm{SL\_TM}}|E_{\mathrm{SL\_TM}}(t)|^2\}, \tag{7}$$

$$\Delta\omega_{\mathrm{inj}} = \omega_{\mathrm{ML\_TE}} - \omega_{\mathrm{SL\_TM}} = 2\pi(f_{\mathrm{ML\_TE}} - f_{\mathrm{SL\_TM}}), \tag{8}$$

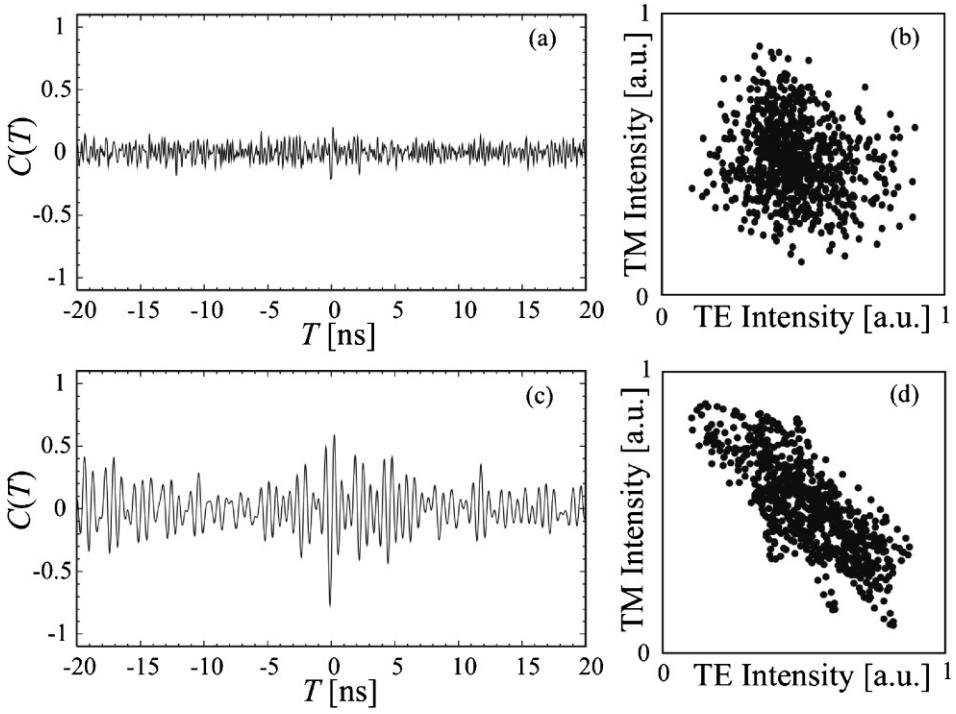

Fig. 4. Experimental results for the correlation between TE and TM modes in receiver laser. (a) Correlation over the entire frequency bandwidth of 0–8 GHz and (b) correlation plot at $T = 0$ ns. (c) Correlation for low-pass filtered signals of 0–2 GHz and (d) correlation plot at $T = 0$ ns.

where the subscript SL indicates the slave receiver laser, κ_{inj} is the injection ratio from the transmitter laser to the receiver laser, and τ_c is the time required for injection from the transmitter laser to the receiver laser. The frequency detuning of the polarization-rotated optical injection from the transmitter laser to the receiver laser, $\Delta\omega_{inj}/2\pi$, is also introduced.

In the following numerical simulations, the same values for the device parameters and the same oscillation conditions were used for both the transmitter and receiver lasers. The gains of the TE and TM modes were set to 0.400×10^{-12} and $0.310 \times 10^{-12}\,m^3\,s^{-1}$, respectively. The difference between the gains of the two modes was set to be almost equal to that used in ref. 12. The difference between the gains plays an important role in the dynamics of polarization-rotated optical feedback. The carrier densities at transparency were assumed to be equal for both polarization modes and were set to $n_0 = 1.40 \times 10^{24}\,m^3\,s^{-1}$. Other parameter values used were a threshold carrier density of $n_{th} = 1.42 \times 10^{24}\,m^3\,s^{-1}$, a carrier lifetime of $\tau_s = 2.04 \times 10^{-9}$ s, a thickness of the active region of $d = 0.2\,\mu m$, a TE-mode oscillation wavelength of the master laser of $\lambda_{ML\_TE} = 782.4053$ nm, a TE-mode oscillation wavelength of the slave laser of $\lambda_{SL\_TE} = 782.4071$ nm, and a linewidth enhancement factor of $\alpha = 3.00$. The laser was biased at $2.0J_{th}$ and the relaxation oscillation frequency of the solitary mode at this injection current was calculated to be 3.66 GHz. The laser operation parameters were chosen to have almost the same relaxation oscillation frequency as that in the experiment. Under these conditions, the power ratio between the TE- and TM-mode oscillations was calculated to be 1000 : 2.

The polarization-rotated optical feedback coefficient in the transmitter laser was $\kappa/\tau_{in} = 0.016 \times 10^{12}\,s^{-1}$ (corresponding to an external intensity reflectivity of 1.06%). The feedback ratio is consistent with that in an experiment when intensity losses for the beam fed back into the active layer are taken into account. This feedback fraction differs from those used in previous numerical simulations.[11–13] The injection coefficient from the transmitter laser to the receiver laser was chosen to be $\kappa_{inj}/\tau_{in} = 0.016 \times 10^{12}\,s^{-1}$, which is equal to the optical feedback ratio in the transmitter laser. We introduced frequency detuning between the two polarization modes: $\Delta f_{ML} = \Delta\omega_{ML}/2\pi = -870$ MHz and $\Delta f_{SL} = \Delta\omega_{SL}/2\pi = -870$ MHz.[16] The same external feedback length as that in the experiment (30 cm) was used, which corresponds to a feedback delay of 2 ns. The receiver laser was located 150 cm from the transmitter laser, so that the injection time was $\tau_c = 5$ ns.

5. Numerical Results

We first present the numerical results for chaos synchronization in semiconductor lasers subjected to polarization-rotated optical feedback and injection. The same frequency bandwidth as that for the experimental data of up to 8 GHz is employed in the numerical simulations. Figures 5(a) and 5(b) respectively show the calculated time series and the corresponding RF spectra of the TE modes in the transmitter and receiver lasers over the entire RF bandwidth when low-pass filtered signals show synchronous oscillations. The two lasers exhibit chaotic oscillations and their spectra contain clear broad peaks corresponding to the relaxation oscillation

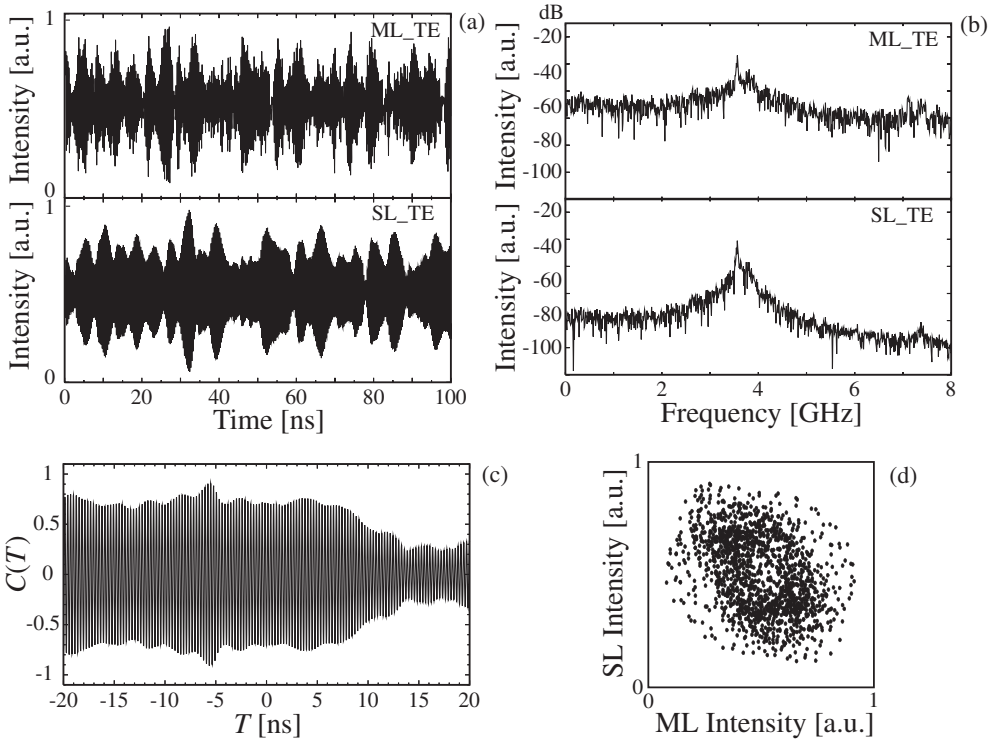

Fig. 5. Numerical results for chaos synchronization. (a) Time series of TE-mode chaotic signals in transmitter and receiver lasers over the entire frequency bandwidth (0–8 GHz). (b) Corresponding RF spectra. (c) Correlation the two waveforms of the master and transmitter TE modes in (a), and (d) correlation plot at $T = -5$ ns.

frequencies. The calculated correlation function for these oscillation states is shown in Fig. 5(c). Figure 5(d) shows the correlation plot at a time delay of $T = -5$ ns, which corresponds to the time of the injection from the transmitter laser to the receiver laser. We were unable to achieve a good correlation at this time offset.

Figure 6 shows the results for synchronous and asynchronous oscillations dependent on the RF components under the same conditions as those for Fig. 5. The same three filter bandwidths as those in the experiments were used. The results for the low-pass filtered signals (0–2 GHz) are shown in the left column. A strong negative correlation peak at a delay time equal to the optical injection ($T = -5$ ns) can be seen in Fig. 6(b), and the correlation coefficient at this time is calculated to be $C(-5) = -0.994$ from the correlation plot in Fig. 6(c). However, a clear correlation is not observable in the plot in Fig. 6(f) for the band-pass filtered signals from 2 to 4.5 GHz. On the other hand, an in-phase correlation is found for the high-pass filtered signals in Fig. 6(i). The correlation coefficient at a time delay of $T = -5$ ns is $C(-5) = 0.828$. These results are reasonably consistent with the experimental ones, although a distinct correlation was not observed for the high-pass filtered signals in the experiments.

Figure 7 shows the band-pass-limited correlations between the TE and TM modes within the receiver laser when the low-pass filtered TE-mode signals of the transmitter and receiver lasers exhibit antiphase chaos synchronization. There is no correlation between the two modes at $T = 0$ ns over the entire frequency bandwidth in Fig. 7(b). However, for the low-pass filtered signals, the two modes oscillate in antiphase with zero time delay ($T = 0$ ns) as shown in Fig. 7(c), and the correlation coefficient is calculated to be $C(0) = -0.993$ from the correlation plot in Fig. 7(d). Although not shown in this paper, the band-pass filtered signals for 2–4.5 GHz exhibit no correlation at $T = 0$ ns. On the other hand, the high-pass filtered signals show an in-phase correlation at $T = 0$ ns, as shown in Fig. 7(e). The correlation coefficient for the high-pass filtered signals calculated from the correlation plot in Fig. 7(f) is $C(0) = 0.848$.

We summarize the mode relations for chaos synchronization in a system with polarization-rotated optical feedback and injection. Figure 8 shows an example for the low-pass filtered case in Fig. 6. Initially, the TM mode of the receiver laser is driven by the TE mode in the transmitter laser. The two modes then show chaotic behavior and the TM mode exhibits antiphase oscillation with the TE mode, as shown in Figs. 8(a) and 8(b). The arrows show an example of corresponding points with synchronous oscillations. The polarization of this chaotic TE mode is rotated by 90° and the beam is injected into the slave receiver laser. The TM mode of the receiver laser is then excited and oscillates in-phase with a delay equal to the transmission time of light, as shown in Fig. 8(d). Then, the TE mode of the receiver laser shows antiphase oscillations relative to the TM mode with a zero time delay as shown in Fig. 8(c). Such example points are also indicated by arrows in Figs. 8(c) and 8(d). As a result, the transmitter and receiver TE modes show anti-

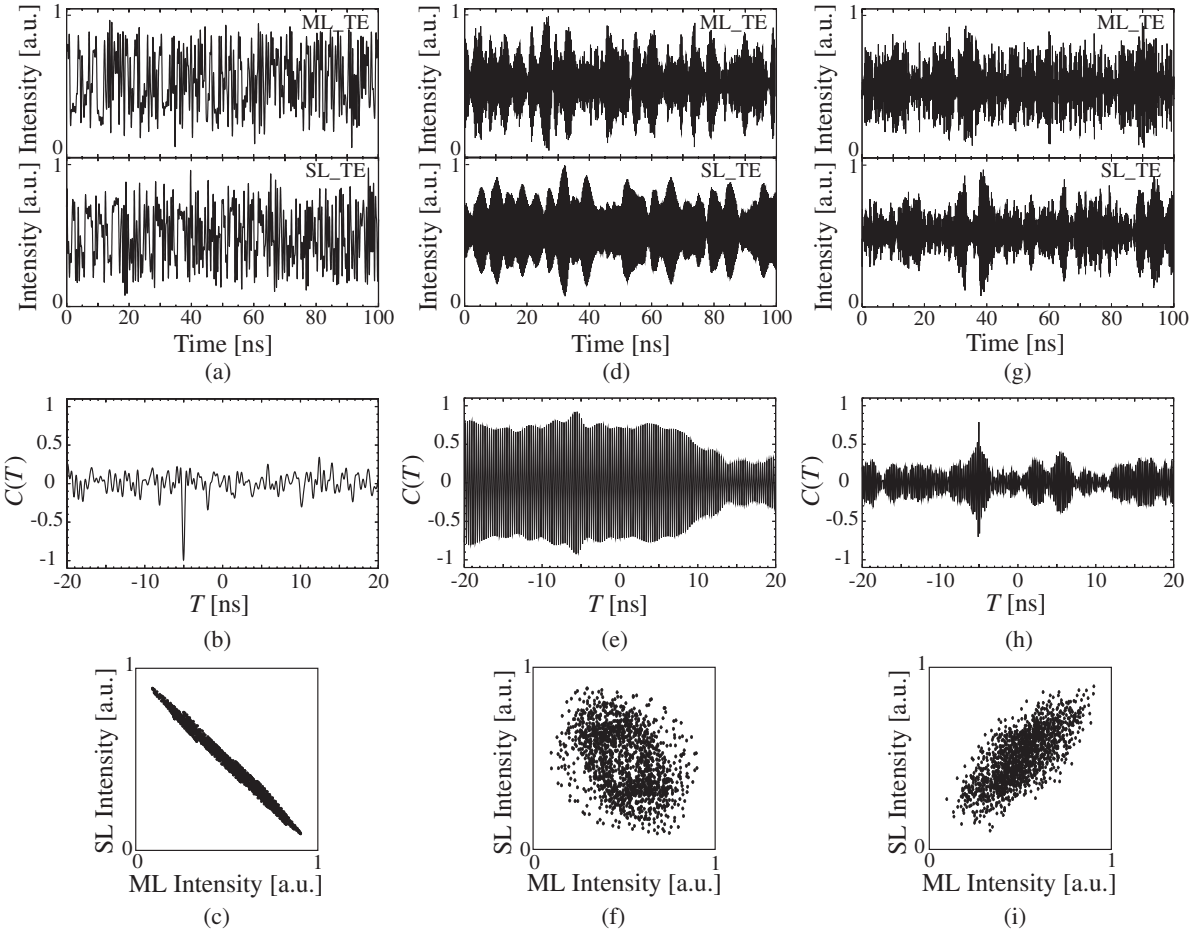

Fig. 6. Numerical results for time series and correlations for band-pass filtered TE-mode signals in transmitter and receiver lasers. Left column: low-pass filtered results (0–2 GHz). Middle column: band-pass filtered results (2.0–4.5 GHz). Right column: high-pass filtered results (4.5–8 GHz). Upper row: Time series of TE modes in transmitter and receiver lasers. Middle row: Correlation betweem waveforms of upper row. Bottom row: Correlation plot at $T = -5$ ns.

phase oscillations with a transmission delay equal to the optical injection time τ_c. For the band-pass filtered signals, we are unable to find distinct mode relations, as has already been discussed.

On the other hand, clear in-phase relations among the modes exist for the high-pass filtered signals as is easily seen from the results in Figs. 6(h) and 6(i). Although the plot is not shown, the mode relation can be explained in a similar manner to the relation in Fig. 8. In this case, the TM mode of the transmitter laser is simply driven by the TE mode without a time delay. The TM mode of the receiver laser is then injected and amplified by the TE mode from the transmitter laser with a transmission delay of τ_c. As a result, the TE mode of the receiver laser is driven by the TM mode of the receiver laser and shows in-phase oscillations with the TE mode of the transmitter laser with a transmission time delay. Namely, for the low-pass filtered signals, the effect of competition between the light powers of the TE and TM mode oscillations is dominant. On the other hand, the effect of drive and response by optical injection dominates for high-pass filtered signals due to injection at a relatively strong optical power.

The change of the dynamics from antiphase to in-phase correlation between the two polarization modes due to polarization-rotated optical feedback and optical injection is an interesting issue. In a previous paper,[13] Sukow *et al.* observed in-phase dynamics for very strong optical feedback, ten times larger than that in our case. The main aim of this paper is to demonstrate the existence of chaos synchronization in a regime of antiphase oscillations between the TE and TM modes in semiconductor lasers. However, in a preliminary numerical study on the transition from antiphase to in-phase dynamics with the increase of the optical feedback and injection levels, in-phase dynamics are always observed at and over $\kappa_{inj}/\tau_{in} = 0.08 \times 10^{12}\,s^{-1}$, which is five times larger than the value in the present experiment. During the transition, there exists a mixed state of anti- and in-phase oscillations in the lower frequency components of the TE and TM modes. Further investigation of this subject is still required. In the experiment, we could not observe in-phase oscillations for the higher-frequency band [Fig. 3(i)]. On the other hand, in-phase oscillation was observed in the numerical simulation [Fig. 6(i)]. A brief discussion of the reason for this discrepancy has already

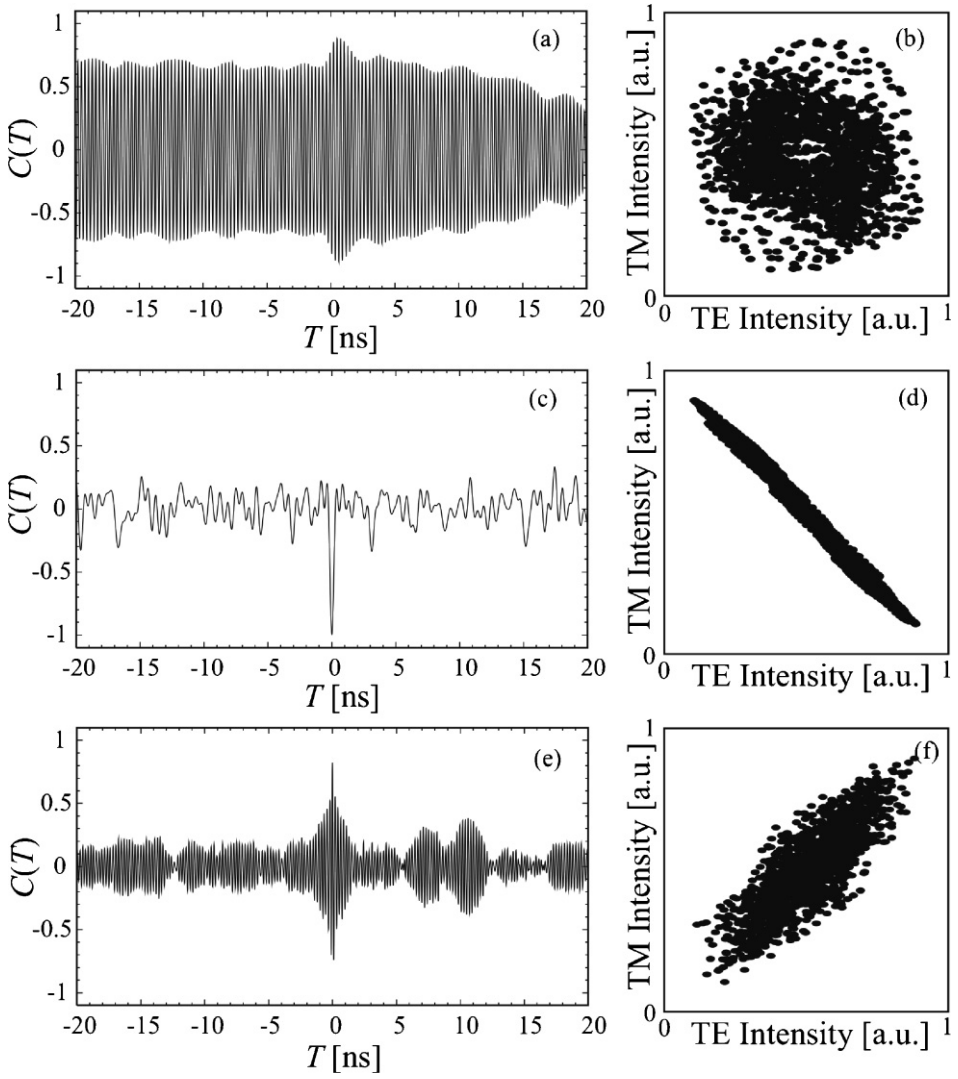

Fig. 7. Numerical results for the correlation between TE and TM modes in receiver laser. (a) Correlation between TE and TM waveforms over the entire bandwidth of 0–8 GHz and (b) correlation plot at $T = 0$ ns. (c) Correlation for low-pass filtered signals of 0–2 GHz and (d) correlation plot at $T = 0$ ns. (e) Correlation for high-pass filtered signals of 4.5–8 GHz and (f) correlation plot at $T = 0$ ns.

been given. Another possible reason is the inclusion of small Langevin noises in the numerical calculation. To avoid over- and underflows in numerical calculations, small Langevin noises are added to the rate equation to mainly see the pure dynamics. Also the limitation of the detector noises and the other limitations of the experimental apparatus are not included in the numerical simulations. Therefore, precise experiments using a sensitive apparatus are also required as a future study.

Finally, we briefly compare the present results for chaos synchronization with those of previous studies. In conventional systems that employ TE–TE coupling for optical feedback in a transmitter laser and TE optical injection into a receiver laser, the slave receiver laser exhibits an in-phase oscillation that synchronizes with the transmitter chaos and the signal delay is either $\tau_c - \tau$ or τ_c, corresponding to perfect or generalized chaos synchronization. Synchronous chaotic oscillations have no RF dependent properties, although the correlation deteriorates slightly for higher RF-components in generalized chaos synchronization.[1)] Furthermore, the synchronization properties are independent of the optical feedback and injection strengths. For polarization-rotated optical feedback and injection, conditions for perfect chaos synchronization or injection synchronization occur when the feedback and injection are sufficiently strong and no frequency detuning exists.[13,14)] Under these conditions, the drive-response nature becomes dominant over the entire frequency range and only in-phase synchronous oscillations between the transmitter and receiver lasers are observed. In the previous studies, the correlations between the polarization modes had no RF-dependent characteristics. In contrast, the effects of competition and injection on mode excitations are mixed in the present moderate polarization-rotated optical feedback and optical injection, which gives rise to RF-dependent dynamics. However, further study is required to determine the origin of these dynamics.

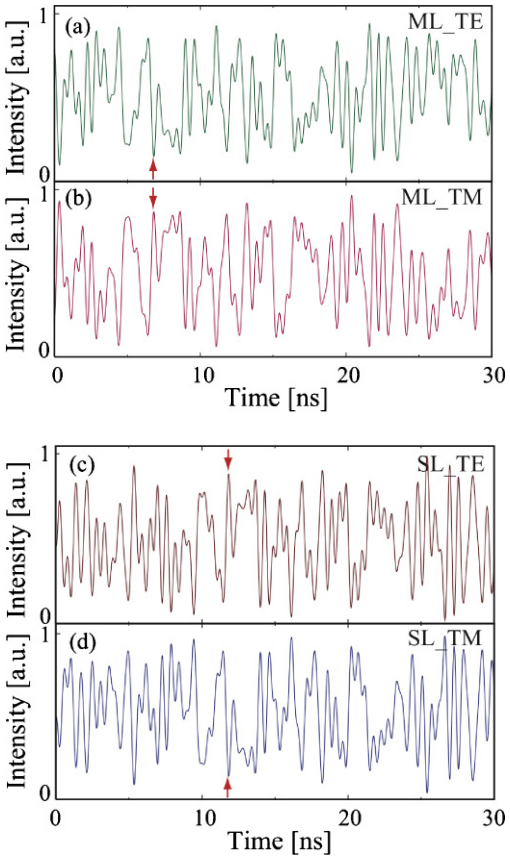

Fig. 8. (Color online) Example of mode relations of chaos synchronization in low-pass filtered signals. Waveforms for (a) transmitter TE mode, (b) transmitter TM mode, (c) receiver TE mode, and (d) receiver TM mode. Corresponding synchronous points of either in-phase or antiphase oscillations are indicated by arrows.

6. Conclusions

We have investigated the synchronization properties of polarization-rotated optical feedback and injection in semiconductor lasers. For moderate optical feedback, the synchronization properties were markedly different from previous results for strong polarization-rotated optical feedback and injection. We have also observed RF-dependent chaos synchronization in accordance with the dynamics on the transmitter side. We have suggested some explanations for the different dynamics and synchronization properties in the present study and previous studies; however, they do not satisfactorily explain the origin of these phenomena. Thus, further study is required on RF-dependent dynamics and chaos synchronization in polarization-rotated optical feedback and injection.

Finally, we comment on the suitability of polarization-rotated optical feedback for chaotic communications. In the early days, a system with polarization-rotated optical feedback was treated as an incoherent system, in which the delayed intensity of the polarization-rotated component was simply described as an intensity feedback to the carrier density in the rate equations. If this assumption is true, locking of the optical carrier frequency should not occur in long-distance chaotic communications using such systems. However, the system must be treated as a coherent model. Consequently, similar problems will occur to those that occur in systems with TE–TE optical feedback and injection in polarization-rotated schemes. Moreover, the dynamics of polarization-rotated optical feedback in semiconductor lasers are so complex that chaos synchronization based on such systems may be less suitable for simple chaotic communications than systems with TE–TE optical feedback and injection.

References

1) J. Ohtsubo: *Semiconductor Lasers: Stability, Instability and Chaos* (Springer, Berlin, 2008) 2nd ed.
2) J. Ohtsubo: IEEE J. Quantum Electron. **38** (2002) 1141.
3) A. Argyris, D. Syvridis, L. Larger, V. Annovazzi-Lodi, P. Colet, I. Fischer, J. Garcia-Ojalvo, C. R. Mirasso, L. Perquera, and K. A. Shore: Nature **438** (2005) 343.
4) K. Otsuka and J. L. Chern: Opt. Lett. **16** (1991) 1759.
5) T.-C. Yen, J.-W. Chang, J.-M. Lin, and R.-J. Chen: Opt. Commun. **150** (1998) 158.
6) J. M. Saucedo Solorio, D. W. Sukow, D. R. Hicks, and A. Gavrielides: Opt. Commun. **214** (2002) 327.
7) R. Ju and P. S. Spencer: J. Lightwave Technol. **23** (2005) 2513.
8) F. Rogister, A. Locquet, D. Pieroux, M. Sciamanna, O. Deparis, P. Mégret, and M. Blondel: Opt. Lett. **26** (2001) 1466.
9) F. Rogister, D. Pieroux, M. Sciamanna, P. Mégret, and M. Blondel: Opt. Commun. **207** (2002) 295.
10) D. W. Sukow, K. L. Blackburn, A. R. Spain, K. J. Babcock, J. V. Bennett, and A. Gavrielides: Opt. Lett. **29** (2004) 2393.
11) D. W. Sukow, A. Gavrielides, T. Erneux, M. J. Baracco, Z. A. Parmenter, and K. L. Blackburn: Phys. Rev. A **72** (2005) 043818.
12) N. Shibasaki, A. Uchida, S. Yoshimori, and P. Davis: IEEE J. Quantum Electron. **42** (2006) 342.
13) D. W. Sukow, A. Gavrielides, T. McLachlan, G. Burner, J. Amonette, and J. Miller: Phys. Rev. A **74** (2006) 023812.
14) A. Gavrielides, T. Erneux, D. W. Sukow, G. Burner, T. McLachlan, J. Miller, and J. Amonette: Opt. Lett. **31** (2006) 2006.
15) T. Heil, A. Uchida, P. Davis, and T. Aida: Phys. Rev. A **68** (2003) 033811.
16) Y. Takeuchi, R. Shogenji, and J. Ohtsubo: Appl. Phys. Lett. **93** (2008) 181105.
17) Y. Takeuchi, R. Shogenji, and J. Ohtsubo: Opt. Rev. **17** (2010) 144.